JTSE - Journal of Tropical Science and Engineering
Volume 1, Issue 3, September 2026
https://doi.org/10.58334/jtse.vol.001.799

# Urea-Functionalized GO-ZnO Nanocomposites for Enhanced Corrosion Protection of Low-Carbon Steel: Roles of Dispersion and Interfacial Adsorption

**Do Tan Tai[(1)]✉, Antonov S.V.[(2)], Bezrukov N.P.[(2)], Makarova V.V.[(2)], Nguyen Thi Thu Hien[(3)], Nguyen Kim Thanh[(4)], Tran Thi Truc Suong[(4)], Duong Huynh Thanh Linh[(4)], Tran Boi An[(4)]**

[(1)]*Southern Branch, Joint Vietnam-Russia Tropical Science and Technology Research Center, Ho Chi Minh City, Vietnam*

[(2)]*A.V. Topchiev Institute of Petrochemical Synthesis, Russian Academy of Sciences, Moscow, Russian Federation*

[(3)]*HCMC University of Industry and Trade, Ho Chi Minh City, Vietnam*

[(4)]*Institute of Advanced Technology, Vietnam Academy of Science and Technology, Ho Chi Minh City, Vietnam*

✉**Corresponding author**

*Email: tantaido77@gmail.com*

*ORCID: 0009-0002-7112-3350*

**How to cite this article**

Do, T. T., Antonov, S. V., Bezrukov, N. P., Makarova, V. V., Nguyen, T. T. H., Nguyen, T. K. T., Tran, T. T. S., Duong, H. T. L., & Tran, B. A. (2026). Urea-Functionalized GO-ZnO Nanocomposites for Enhanced Corrosion Protection of Low-Carbon Steel: Roles of Dispersion and Interfacial Adsorption. *Journal of Tropical Science and Engineering*, *15*(3), 43-55. https://doi.org/10.58334/jtse.vol.001.799

**Abstract**

In this work, a series of urea-modified GO-ZnO (U-GO-ZnO) hybrid materials were synthesized by modifying GO-ZnO nanocomposites with urea to enhance their anti-corrosive performance in saline environments. The incorporation of urea improves surface functionalization, interfacial interaction, and dispersion stability of GO-ZnO, thereby enhancing its protective performance on metallic substrates. The prepared GO-ZnO material was successfully modified with 3 wt.% urea, and the resulting U-GO-ZnO composites were systematically characterized using Fourier-transform infrared spectroscopy (FTIR), X-ray diffraction (XRD), scanning electron microscopy (SEM), and Raman spectroscopy. FTIR and Raman analyses confirmed the chemical interaction between urea and oxygen-containing functional groups on the GO surface, while XRD patterns revealed the preserved crystalline structure of ZnO after modification. SEM micrographs showed a more uniform surface morphology and improved particle dispersion, supporting the positive role of urea functionalization. The anti-corrosion performance of U-GO-ZnO was evaluated using both the weight-loss method and potentiostatic polarization measurements under varying inhibitor concentrations and immersion durations. The results demonstrated that exposure time has a significant influence on corrosion inhibition efficiency. In a 3.5 wt.% NaCl solution, the concentration of 0.05 g/L exhibited the most promising inhibition efficiency, reaching 77.73%, 69.01%, and 87.21% after 30, 60, and 120 min, respectively. Furthermore, Nyquist impedance plots obtained by electrochemical impedance spectroscopy (EIS) revealed that electrodes immersed in 0.2 g/L U-GO-ZnO solution possessed the largest charge-transfer resistance, indicating the formation of a highly stable passive layer that effectively mitigates corrosion processes. These findings support the conclusion that urea-modified GO–ZnO is a promising anti-corrosive additive for metal protection applications.

**Keywords**

*Anti-corrosion, graphene oxide, hybrid material, potentiodynamic polarization, zinc oxide.*



## Introduction

Corrosion, caused by chemical or electrochemical reactions at the material surface, leading to material degradation, is regarded as one of the most critical issues in many industries (Necolau & Pandele, 2020). According to the National Association of Corrosion Engineers, the financial loss caused by corrosion is equivalent to 3-5 % of the world's global gross domestic product (GDP) (Chen *et al.*, 2022; Wang *et al.*, 2024). To protect the material and reduce corrosion damage, one of the most effective methods is to apply a coating on the material surface. The conventional anticorrosive coatings, using heavy metals and fossil-based polymers, have been improved with green nanocoating or green nanocomposite materials (He *et al.*, 2019; Nedal *et al.*, 2015). The superior performance of these materials is mainly attributed to the improved structure and morphology at the nanoscale phase (Nguyen *et al.*, 2018).

Graphene is a two-dimensional (2D) material with an sp2-hybridized carbon structure and exceptional properties such as high mechanical flexibility, superior electrical and thermal conductivities, large specific surface area, and high chemical stability (Giannakopoulou *et al.*,

2020; Miyaji *et al.*, 2022). However, one of the major drawbacks of graphene is its poor solubility, which limits its application in either organic solvents or inorganic solvents. One of the possible methods to improve the solubility is the oxidation of graphene to obtain graphene oxide (GO). Since GO has large quantities of oxygen−containing groups such as carboxyl, carbonyl, and hydroxyl/epoxy, it can easily provide various types of functionalization pathways with organic and inorganic materials by covalent/non-covalent functionalization (Sodeinde *et al.*, 2022). However, the closely packed structures of GO nanosheets limit their applications as coating nanofillers because of particle agglomeration and limit the diffusion of corrosive species (George & Ishida, 2018). To improve these problems, recent studies have focused on applying GO nanosheets with nano-metal oxide particles (El Maghrabi *et al.*, 2016).

ZnO is one of the numerous transition metal oxides and has good electrochemical behavior, eco-friendliness, good mechanical stability, and good corrosion protection on metals and alloys (Aryanto *et al.*, 2020). By combining GO and ZnO, researchers aim to create nanocomposites with enhanced performance and tailored properties. Recent studies reported that GO-ZnO nanocomposite showed superhydrophobic, durability, high water contact angle, and corrosion protection (Mohamed *et al.*, 2021).

This work aims to functionalize the GO-ZnO hybrid material through urea modification, and the attachment of -$NH_2$ groups onto its surface, thereby enhancing its compatibility with conventional solvents and coating systems. To achieve this objective, GO-ZnO and U-GO-ZnO were synthesized and systematically characterized using XRD, FTIR, Raman spectroscopy, and SEM to analyze their structural, chemical, and morphological properties. Furthermore, the corrosion inhibition performance of these materials was evaluated using potentiodynamic polarization measurements in 3.5 wt.% NaCl solution, with mild steel electrodes serving as the working electrode. This approach enables a quantitative evaluation of corrosion inhibition efficiency and provides a deeper understanding of the underlying inhibition mechanisms at the metal interface. The obtained results provide valuable insights into the role of surface-functionalized GO-ZnO nanocomposites in enhancing barrier properties and suppressing electrochemical corrosion processes. Consequently, this study contributes to the rational design and optimization of GO-based nanocomposite with improved interfacial compatibility and enhanced anticorrosion performance in aggressive environments.

## Materials and Methods

### *Materials*

Potassium permanganate ($KMnO_4$, 99.5%), concentrated sulfuric acid ($H_2SO_4$, 98 wt.%), phosphoric acid ($H_3PO_4$, analytical purity), hydrogen peroxide ($H_2O_2$), zinc acetate dihydrate ($(CH_3COO)_2Zn.2H_2O$, 99%), urea ($CH_4N_2O$, 99%), and sodium chloride (NaCl, 99%), were of analytical grade and purchased from HiMedia, India. Graphite powder (99%) and urea were supplied by Merck, and de-ionized water was used for all solution preparations.

Graphene oxide (GO) was synthesized from graphite powder using the modified Hummer method and was described as follows. Exactly 2.0 g of graphite was slowly dispersed into 120 mL of mixture of $H_2SO_4/H_3PO_4$ (9:1, v/v) in an ice bath to maintain the temperature at about 4ºC. Then, 0.5 g of $KMnO_4$ (mass ratio $m_{graphite}/m_{KMnO4}$ = 4/1) was slowly added to the mixture with strong magnetic stirring. The reaction mixture was heated and kept at 50ºC for 4 hours until a dark green sludge was obtained. After that, the mixture was diluted by slowly adding 230 mL of de-ionized water, and kept at 90ºC for 8 hours for complete oxidation of graphite. The remaining $KMnO_4$ was completely reduced by 1–2 mL of $H_2O_2$. The mixture was neutralized many times with de-ionized water using a centrifugation, and finally, freeze-dried to obtain dark brown GO powder.

### *Synthesis of graphene oxide-ZnO hybrid material*

First, 0.1 g of GO was dispersed in 100 mL of deionized water and ultrasonicated to obtain a homogeneous dispersion. At the same time, a 0.1 M solution of $(CH_3COO)_2Zn$ was prepared by dissolving $(CH_3COO)_2Zn.2H_2O$ into 100 mL

of deionized water. Then, $(CH_3COO)_2Zn$ was added dropwise into the GO solution at a speed of 3 mL/min and stirred well with a magnetic stirrer. Next, the mixture was alkalized by slowly adding 0.2 M NaOH until pH 11 to obtain the GO-ZnO mixture. The mixture was subjected to hydrothermal treatment at 90°C for 8 hours. The resulting GO-ZnO precipitate was neutralized with de-ionized water by centrifugation, and then dried in a vacuum dryer at 60ºC for 8 hours. GO-ZnO material was characterized by using FTIR, XRD, SEM, and Raman methods. In this experiment, GO-ZnO material was synthesized with a ZnO/GO ratio of 20:1 (w/w).

***Modification of GO-ZnO with urea***

Approximately 0.5 g of synthesized GO-ZnO was ultrasonicated in 50 mL of deionized water. Then, 10 mL of the 3% urea solution was added dropwise into the GO-ZnO solution to obtain a well-mixed solution, then heated and maintained at 80ºC for 6 hours. The resulting U-GO-ZnO precipitate was neutralized with de-ionized water by centrifugation, and then dried in a vacuum dryer at 60ºC for 8 hours.

***Characterization of synthesized materials***

The chemical properties and structure of synthesized GO-ZnO and U-GO-ZnO were characterized by FTIR (wavenumber from 400 to 4000 $cm^{-1}$, scanning step of 8 $cm^{-1}$, and 64 scans, Tensor 27, Bruker, Germany); XRD (2θ from 2-70°, scan rate of 2°/min, Bruker Advance D8, Germany); SEM images (Jeol 6400, Japan); and Raman spectroscopy (532 nm, 25 mW, 100−4000 $cm^{-1}$).

***Analysis of corrosion inhibition performance of U-GO-ZnO using the weight loss method***

GOST 380-89 steel samples (Φ 6 × 50 mm) with an average mass of 11.2 ± 0.25 g were used to evaluate corrosion behavior by the weight loss method. The samples were immersed in 50 mL of 3.5 wt.% NaCl solution in the absence and presence of GO-ZnO and U-GO-ZnO at concentrations of 0.025, 0.05, and 0.1 wt.%. Prior to testing, all specimens were mechanically polished using abrasive papers (grit sizes 800, 1200, and 2000), rinsed with distilled water, washed with ethanol, and dried. The dimensions of each sample were measured to determine the exposed surface area (S). The initial mass ($m_0$) was recorded using an analytical balance with an accuracy of ± 0.0001 g. The samples were then immersed for 3, 5, 10, and 30 days. After each exposure period, the specimens were removed, cleaned to eliminate corrosion products, rinsed, dried, and weighed again (m). The corrosion rate (V) and corrosion inhibition efficiency (H) were calculated using the following equations:

$$V = (m_0 - m) / (S \times t) \quad (mg \cdot cm^{-2} \cdot day^{-1}) \qquad (1)$$

$$H = (V_0 - V) / V_0 \times 100 \quad (\%) \qquad (2)$$

where H is the corrosion inhibition efficiency (%); $V_0$ and V are the corrosion rates of GOST 380-89 steel in 3.5 wt.% NaCl solution in the absence and presence of the inhibitor, respectively, expressed in $mg \cdot cm^{-2} \cdot day^{-1}$.

***Analysis of anti-corrosion property of U-GO-ZnO using potentiodynamic polarization method***

This research has used the potentiodynamic polarization method to evaluate the anti-corrosion property performed on a three-electrode system connected to the Biologic VSP300 (scan rate of 0.1 mV/s, potential range of 50 mV, frequency range from 100 KHz−10 mHz). The three-electrode system includes: the working electrode is an epoxy-casted steel bar exposed to 3.5 wt.% NaCl with/without synthesized materials, the reference electrode is a saturated Ag/AgCl (KCl) electrode, and the counter electrode is a platinum electrode. The $i_{corr}$, $E_{corr,}$ and Tafel slope coefficients $\beta_a$, $\beta_c$ were determined using the Tafel extrapolation method. The study was conducted under various exposure times and concentrations of the synthesized materials.

The interaction of GO-ZnO and U-GO-ZnO with the metallic surface is primarily governed by a strong adsorptive inhibition mechanism coupled with surface passivation. In 3.5 wt.% NaCl solution, these materials adsorb onto the steel surface via electrostatic interactions and coordination between functional groups (–OH, –COOH, $–NH_2$) and Fe atoms, forming a compact protective barrier. This layer effectively blocks active corrosion sites and suppresses both anodic and cathodic reactions.

Simultaneously, the corrosion process induces the formation of a dense iron oxide passive film, whose stability is significantly enhanced by the presence of these materials. This synergistic effect markedly reduces charge transfer and the corrosion rate.

## Results

### *Modification of GO-ZnO with urea*

The interactions between GO and ZnO, as well as between GO-ZnO and urea are shown on the FTIR spectra in Fig. 1a. The infrared spectrum of GO-ZnO shows the stretching vibrations of –OH, C = C, and C–O with the adsorption peaks at 3417, 1588, and 1384 $cm^{-1}$, which belong to the GO hexagonal lattice structure. Besides, the FTIR spectrum of GO-ZnO exhibits a strong peak at 502 $cm^{-1}$ corresponding to the stretching vibration of the Zn-O bond.

The Raman spectra of GO-ZnO and U-GO-ZnO provide important insights into their structural characteristics. As shown in Fig. 1b, the Raman spectrum of GO-ZnO exhibits two prominent peaks at approximately 1337 and 1589 $cm^{-1}$, corresponding to the D and G bands of graphene oxide, respectively. The D band is associated with structural defects and disorder, while the G band reflects the in-plane vibration of $sp^2$-bonded carbon atoms (Yang *et al.*, 2009). In addition, characteristic peaks at 329, 440, and 584 $cm^{-1}$ are attributed to the vibrational modes of ZnO, confirming the successful incorporation of ZnO into the GO matrix.

For U-GO-ZnO, the Raman spectrum retains all key features of GO-ZnO, with D and G bands observed at approximately 1330 and 1589 $cm^{-1}$. Notably, the D-band intensity of U-GO-ZnO is significantly higher than that of GO-ZnO (605.19 vs. 369.29 counts) and exhibits a slight blue shift, indicating an increased degree of structural disorder after urea modification. Similarly, the G-band intensity is also enhanced (502.62 vs. 348.04 counts), suggesting changes in the electronic structure and improved interaction within the material. Furthermore, both GO-ZnO and U-GO-ZnO display 2D bands at approximately 2878 and 2926 $cm^{-1}$, confirming the preservation of the graphene-based structure after modification (Bai *et al.*, 2015).

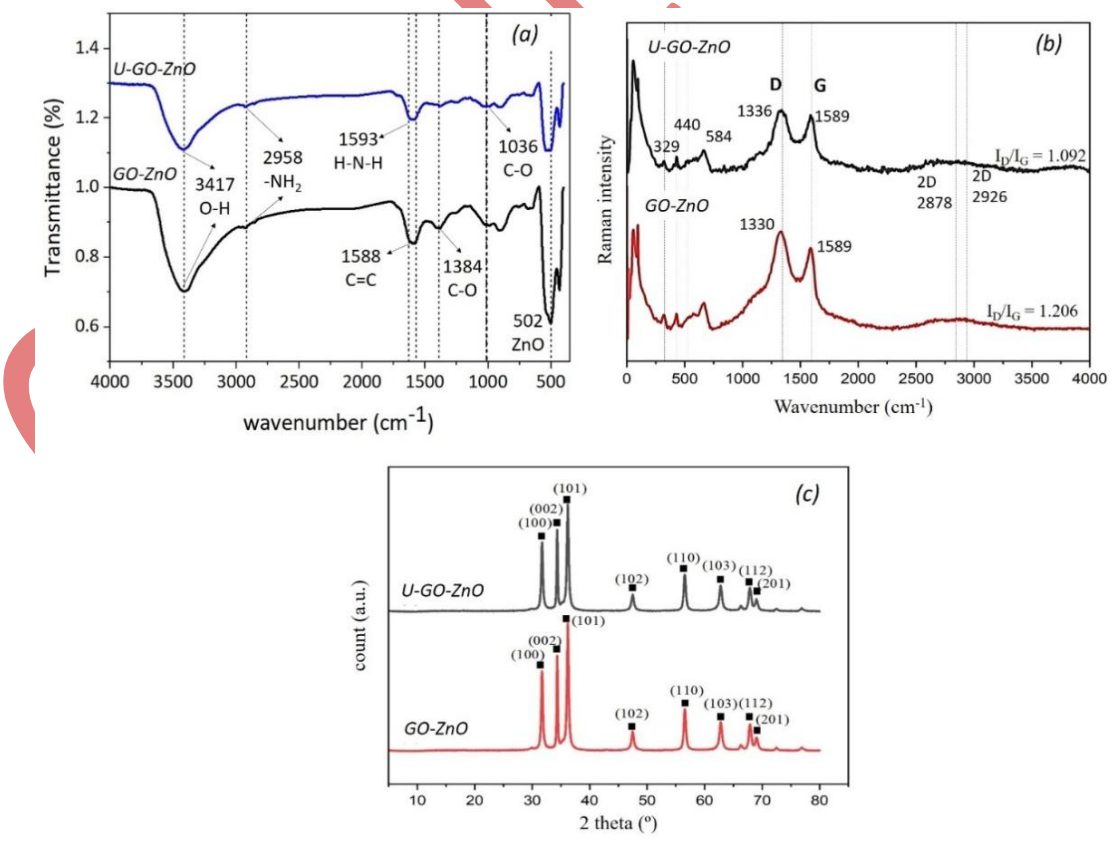


Figure 1. FTIR spectra (a), Raman spectra (b), and X-ray diffraction patterns (c) of U-GO-ZnO and GO-ZnO.

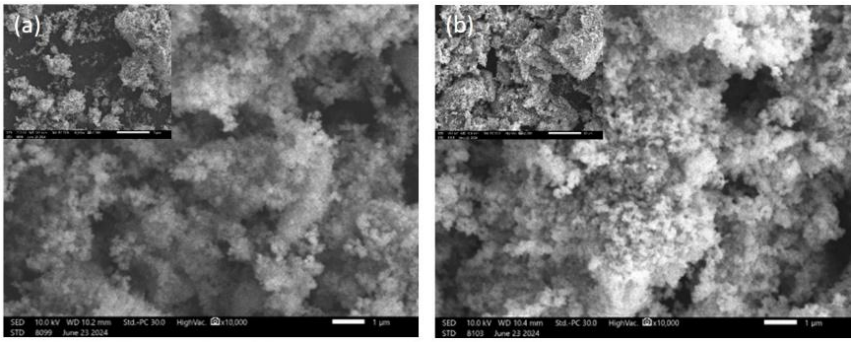


Figure 2. SEM image of hybrid material GO-ZnO (a), and modified material U-GO-ZnO (b) at magnification ×2500 and ×10000.

The XRD patterns of both GO-ZnO and U-GO-ZnO (Fig. 1c) show the characteristic diffraction of wurtzite-structured ZnO, consistent with JCPDS No. 36−1451. The 2θ values at 32°, 35°, 37°, 48°, 57°, 63°, 68°, and 69° correspond to the diffraction planes (100), (002), (101), (102), (110), (103), (112), and (201). The SEM images in Figure 2 show that both GO-ZnO and U-GO-ZnO exhibit flake-like structures (with a diameter of approximately 100 nm), high porosity, and a tendency to agglomerate. The morphology of the U-GO-ZnO samples remains similar to that of GO-ZnO, confirming that the urea modification does not alter the crystalline structure observed in the XRD results.

***Anti-corrosion performance of U-GO-ZnO with loss weight method***

The results in Table 1 show a general decrease in corrosion rate with increasing immersion time for all systems, likely due to the gradual formation of corrosion products or partially protective surface films. Compared to the blank 3.5 wt.% NaCl solution, the addition of GO-ZnO at low concentrations (0.05 and 0.1 g/L) leads to a slight reduction in the corrosion rate, indicating a modest inhibition effect attributed to the barrier properties and surface adsorption of the nanocomposite. However, the inhibition efficiency remains limited over extended immersion times, suggesting that the protective layer is not sufficiently stable.

At a higher concentration (0.2 g/L GO-ZnO), a different trend is observed: while initial corrosion rates decrease slightly at 3–5 days, they become higher than the blank after 10–30 days. This behavior may result from nanoparticle agglomeration, leading to poor dispersion and the formation of defects that facilitate the penetration of corrosive species. Furthermore, the increased mass loss observed after 30 days may be associated with the destabilization and subsequent detachment of loosely bound corrosion products or protective films, exposing fresh metal surfaces to the electrolyte. This phenomenon, combined with possible pitting corrosion induced by chloride ions, results in an acceleration of the corrosion process at longer exposure times. These findings highlight the critical role of nanocomposite dispersion and optimal concentration in achieving effective and durable corrosion inhibition.

The corrosion rates in Table 1 indicate that U-GO-ZnO exhibits a concentration-dependent inhibition behavior over time. At low concentrations (0.05 and 0.1 g/L), the corrosion rate decreases initially, with values of 42.53–33.86 and 46.25–29.07 $mg.cm^{-2}.day^{-1}$ over 3–30 days, respectively, suggesting a moderate protective effect during the early immersion period (3–10 days). However, similar to the GO-ZnO, the inhibition performance at these concentrations does not significantly improve at longer exposure times, implying that the protective layer formed is relatively unstable or insufficiently compact.

In contrast, at a higher concentration (0.2 g/L), U-GO-ZnO demonstrates a more pronounced and sustained anticorrosion effect, with corrosion rates continuously decreasing to 26.84 $mg.cm^{-2}.day^{-1}$ after 30 days. This enhanced performance can be attributed to improved surface coverage and stronger interaction between the $–NH_2$ -functionalized nanocomposite and the steel substrate, leading to the formation of a more uniform and stable barrier layer. These results highlight the beneficial role of surface functionalization and optimal loading in improving long-term corrosion protection.

**Table 1. Corrosion rate (mg·cm$^{-2}$·day$^{-1}$) and corrosion inhibition efficiency (η, %) of GO-ZnO and U-GO-ZnO in 3.5 wt.% NaCl solution at different immersion times**

| Sample | Corrosion rate (mg.cm$^{-2}$.day$^{-1}$) | | | | η (%) | | | |
|---|---|---|---|---|---|---|---|---|
| | 3 days | 5 days | 10 days | 30 days | 3 days | 5 days | 10 days | 30 days |
| 3.5 wt.% NaCl | 53.6 | 49.89 | 54.45 | 58.74 | - | - | - | - |
| 0.05 GO-ZnO | 42.15 | 36.7 | 30.11 | 33.28 | 21.36 | 26.44 | 44.70 | 43.34 |
| 0.1 GO-ZnO | 45.02 | 37.9 | 33.81 | 33.16 | 16.01 | 24.03 | 37.91 | 43.55 |
| 0.2 GO-ZnO | 41.9 | 36.72 | 32.5 | 31.8 | 21.83 | 26.40 | 40.31 | 45.86 |
| 0.05 U-GO-ZnO | 45.11 | 35.12 | 30.69 | 31.61 | 15.84 | 29.61 | 43.64 | 46.19 |
| 0.1 U-GO-ZnO | 44.6 | 35.79 | 30.93 | 30.78 | 16.79 | 28.26 | 43.19 | 47.60 |
| 0.2 U-GO-ZnO | 45.51 | 35.93 | 31.04 | 31.84 | 15.09 | 27.98 | 42.99 | 45.79 |

***Study of anti-corrosion performance using the kinetic potentiodynamic polarization method***

The corrosion inhibition performance of GO-ZnO was systematically studied using potentiodynamic polarization measurements at concentrations of 0.05-0.2 g/L and exposure times of 30-120 min (Figure 3). At the initial 30 mins, the corrosion potential $E_{corr}$ shifts to -711, -835, and -720 mV vs. Ag/AgCl (KCl) for 0.05, 0.1, and 0.2 g/L, respectively, indicating a concentration-dependent electrochemical response. After 60 min, a negative shift in $E_{corr}$ (-863 to -901 mV vs. Ag/AgCl (KCl)) is observed, suggesting enhanced adsorption of inhibitor species and the steel surface, likely due to adsorption and the gradual formation of a passivation layer. However, at a longer exposure time (120 min), $E_{corr}$ shifts back toward less negative values (-674 and -730 mV vs. Ag/AgCl (KCl) for 0.05 and 0.1 g/L), implying stabilization of the surface and the establishment of a more compact inhibitive film. This trend reflects a dynamic inhibition mechanism, where initial adsorption is followed by film restructuring and densification. Overall, the results suggest that GO-ZnO exhibits time and concentration-dependent inhibition behavior, with improved performance associated with the formation of a stable barrier layer that limits charge transfer and corrosion reactions.

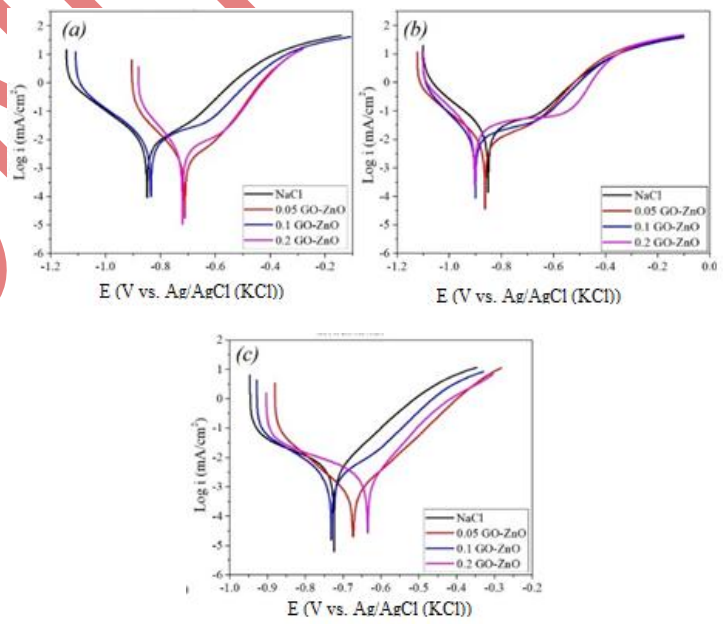


Figure 3. Potentiodynamic polarization curve of GOST 380-89 steel electrode in 3.5 wt.% NaCl solution containing GO-ZnO material, exposure time 30 min (a), 60 min (b), and 120 min (c). E (V vs. Ag/AgCl (KCl)).

Table 2 shows that GO-ZnO effectively reduces the $i_{corr}$ after 30 min, confirming its inhibition performance. The blank solution exhibits a high $i_{corr}$ of 15.843 µA/cm², while the addition of 0.05 and 0.2 g/L GO-ZnO cause the decrease of $i_{corr}$ to 7.759 and 13.352 µA/cm², respectively. The stronger inhibition at 0.05 g/L suggests better dispersion and surface passivation, whereas slight aggregation at higher concentration may reduce efficiency. The decrease in $i_{corr}$ indicates suppressed charge transfer, primarily through inhibition of the cathodic reaction, likely due to the formation of an adsorbed protective layer that limits oxygen diffusion and corrosion kinetics.

**Table 2. Electrochemical parameters determined by Tafel extrapolation of the potentiodynamic polarization curve measured on the GOST 380-89 steel electrode exposed in 3.5 wt.% NaCl solution without/with GO-ZnO**

| Material | Concentration (g/L) | $E_{corr}$ (mV vs. Ag/AgCl (KCl)) | $i_{corr}$ (µA/cm²) | $\beta_a$ (mV/Dec) | $\beta_c$ (mV/Dec) | η (%) |
|---|---|---|---|---|---|---|
| ***After 30 min*** | | | | | | |
| **Blank** | | -889 | 15.843 | 264.9 | 107.7 | – |
| **GO-ZnO** | 0.05 | -884 | 7.759 | 256.4 | 89.7 | 51.03 |
| | 0.10 | -835 | 12.088 | 321.7 | 145.7 | 23.70 |
| | 0.20 | -890 | 13.352 | 368.0 | 108.4 | 15.72 |
| ***After 60 min*** | | | | | | |
| **Blank** | | -872 | 18.516 | 282.1 | 109.9 | – |
| **GO-ZnO** | 0.05 | -863 | 12.892 | 273.3 | 125.5 | 30.37 |
| | 0.10 | -867 | 12.088 | 307.6 | 113.8 | 34.72 |
| | 0.20 | -884 | 13.490 | 277.5 | 104.1 | 27.14 |
| ***After 120 min*** | | | | | | |
| **Blank** | | -853 | 27.884 | 354.5 | 136.5 | – |
| **GO-ZnO** | 0.05 | -871 | 12.227 | 342.0 | 114.7 | 56.15 |
| | 0.10 | -901 | 11.515 | 335.5 | 104.3 | 58.70 |
| | 0.20 | -902 | 22.639 | 348.6 | 108.9 | 18.81 |

The potentiodynamic polarization curve of the steel electrode after 30, 60, and 120 minutes of immersion in a solution containing GO-ZnO is shown in Figure 4. The potentiodynamic polarization curve of the steel electrode exposed to the GO-ZnO solution for 30 minutes tends to shift to a more positive potential compared to the blank solution, while it tends to shift to a more negative potential after 60 min and 120 min. All the electrochemical parameters were determined by Tafel extrapolation of the potentiodynamic polarization curves using EC-LAB software ver.10.36.

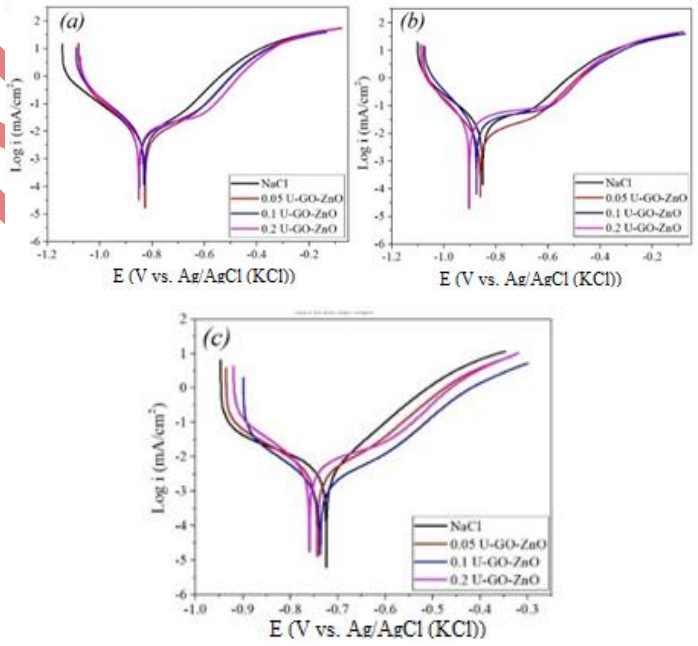


Figure 4. Potentiodynamic polarization curve of GOST 380-89 steel electrode in 3.5 wt.% NaCl solution with 0.05 g/L GO-ZnO and 0.05, 0.1, and 0.2 g/L U-GO-ZnO at 30 min (a), 60 min (b), 120 min (c).

Table 3 shows a clear dependence of corrosion inhibition on both concentration and exposure time for U-GO-ZnO. At 30 min, the blank solution exhibits a high $i_{corr}$ of 15.843 µA/cm², while the addition of U-GO-ZnO reduces $i_{corr}$ to 5.748, 10.661, and 11.028 µA/cm² at 0.05, 0.1, and 0.2 g/L, corresponding to inhibition efficiencies of 63.72%, 32.71%, and 30.39%, respectively. This indicates that the lowest concentration (0.05 g/L) provides the most effective initial inhibition, likely due to better dispersion and rapid adsorption on the steel surface.

However, with increasing immersion time, the inhibition performance of 0.1 g/L improves significantly, reaching 50.79% and 83.22% after 60 and 120 min, respectively. This trend suggests the gradual formation and stabilization of a protective film on the steel surface. Overall, while lower concentration favors immediate inhibition, moderate concentration (0.1 g/L) provides superior long-term corrosion protection.

In general, the inhibition mechanism of GO-ZnO and U-GO-ZnO can be interpreted based on the variation of $i_{corr}$, $E_{corr}$, and cathodic and anodic Tafel slopes including ($\beta_a$ and $\beta_c$). A predominant change in the $\beta_c$ with relatively minor variation in the $\beta_a$ indicates a cathodic inhibition mechanism, where the inhibitor suppresses the oxygen reduction reaction. This behavior is consistent with the observed decrease in $i_{corr}$ at low concentrations, suggesting effective blocking of cathodic active sites. In contrast, if $\beta_a$ is more significantly affected, the inhibitor acts on the anodic dissolution of Fe ion. In cases where both $\beta_a$ and $\beta_c$ are altered and $E_{corr}$ shows only slight shifts (typically < 85 mV), the inhibitor is classified as a mixed-type inhibitor. Based on the results, the GO-ZnO systems exhibit predominantly cathodic inhibition at early stages, while U-GO-ZnO shows a transition toward mixed-type behavior over time, reflecting the formation of a more uniform and stable protective film.

**Table 3. Electrochemical parameters determined by Tafel extrapolation of the potentiodynamic polarization curve measured on the GOST 380-89 steel electrode in 3.5 wt.% NaCl solution without/with U-GO-ZnO**

| Material | Concentration (g/L) | $E_{corr}$ (mV vs. Ag/AgCl (KCl)) | $i_{corr}$ (µA/cm$^2$) | $\beta_a$ (mV/Dec) | $\beta_c$ (mV/Dec) | η (%) |
|---|---|---|---|---|---|---|
| ***After 30 min*** | | | | | | |
| **Blank** | | -889 | 15.843 | 264.9 | 107.7 | – |
| **GO-ZnO** | 0.05 | -884 | 7.759 | 256.4 | 89.7 | 51.03 |
| | 0.05 | -826 | 5.748 | 189.7 | 117.3 | 63.72 |
| **U-GO-ZnO** | 0.10 | -870 | 10.661 | 285.8 | 116.8 | 32.71 |
| | 0.20 | -850 | 11.028 | 368.6 | 114.9 | 30.39 |
| ***After 60 min*** | | | | | | |
| **Blank** | | -872 | 18.516 | 282.1 | 109.9 | – |
| **GO-ZnO** | 0.05 | -863 | 12.892 | 273.3 | 125.5 | 30.37 |
| | 0.05 | -861 | 8.647 | 269.9 | 99.5 | 53.30 |
| **U-GO-ZnO** | 0.10 | -830 | 9.112 | 233.2 | 121.7 | 50.79 |
| | 0.20 | -760 | 4.843 | 178.8 | 91.2 | 73.84 |
| ***After 120 min*** | | | | | | |
| **Blank** | | -853 | 27.884 | 354.5 | 136.5 | – |
| **GO-ZnO** | 0.05 | -871 | 12.227 | 342.0 | 114.7 | 56.15 |
| | 0.05 | -756 | 5.487 | 225.8 | 106.5 | 80.32 |
| **U-GO-ZnO** | 0.10 | -758 | 4.679 | 237.0 | 84.2 | 83.22 |
| | 0.20 | -752 | 5.319 | 205.8 | 97.4 | 80.92 |

***Study of the EIS total impedance***

The Nyquist impedance spectra of the electrodes investigated in 3.5 wt.% NaCl solution containing GO-ZnO and U-GO-ZnO materials is shown in Figure 5a. Accordingly, the recorded Nyquist plots exhibit a single semicircular arc at high frequencies, with no evidence of a second arc. This indicates that the materials dispersed in the NaCl solution are adsorbed onto the electrode surface, forming a protective barrier layer that limits the corrosion process. The results of electrochemical parameter analysis based on the equivalent circuit diagram in Figure 5d are presented in Table 4.

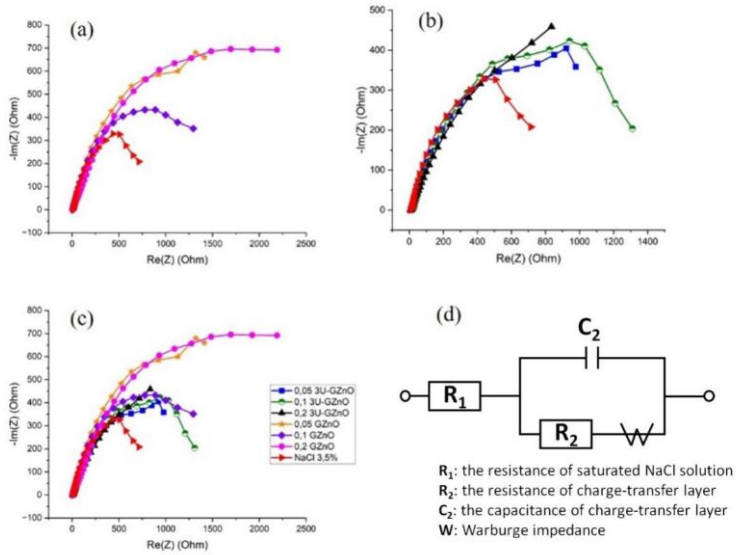


Figure 5. Impedance spectrum of GOST 380-89 steel electrode in 3.5 wt.% NaCl solution with GO-ZnO (a), U-GO-ZnO (b), comparing both materials (c) with three corresponding concentrations of 0.05, 0.1, and 0.2 g/L for 120 min; equivalent circuit diagram (d).

**Table 4. Electrochemical parameters determined by impedance spectrum of GOST 380-89 steel electrode in 3.5 wt.% NaCl solution in the presence of GO-ZnO and U-GO-ZnO materials; characterized time is 120 min.**

| Material | $R_1$ (Ω) | $R_2$ (Ω) | $C_2$ (μF) |
|---|---|---|---|
| 3.5 wt.% NaCl | 6.75 | $2.53 \times 10^{-1}$ | $7.09 \times 10^{-10}$ |
| 0.05 GO-ZnO | 6.15 | $2.25 \times 10^{0}$ | $31.39 \times 10^{0}$ |
| 0.1 GO-ZnO | 6.15 | $4.79 \times 10^{-1}$ | $3.61 \times 10^{-11}$ |
| 0.2 GO-ZnO | 6.96 | $1.13 \times 10^{0}$ | $7.69 \times 10^{-13}$ |
| 0.05 U-GO-ZnO | 4.64 | $6.02 \times 10^{-1}$ | $7.04 \times 10^{-11}$ |
| 0.1 U-GO-ZnO | 7.04 | $1.30 \times 10^{0}$ | $4.14 \times 10^{0}$ |
| 0.2 U-GO-ZnO | 5.76 | $7.80 \times 10^{-1}$ | $2.84 \times 10^{0}$ |

The $R_2$ parameter represents the resistance of the surface passive layer formed at the electrode/electrolyte interface and is a key indicator of corrosion protection performance. As shown in Table 4, the blank 3.5 wt.% NaCl solution exhibits a relatively low $R_2$ value of $2.53 \times 10^{-1}$ Ω, reflecting the formation of a weak and unstable passive layer. Upon the addition of GO-ZnO, the $R_2$ values increase to $2.74 \times 10^{-1}$, $4.79 \times 10^{-1}$, and $3.06 \times 10^{-1}$ Ω at concentrations of 0.05, 0.1, and 0.2 g/L, respectively, indicating an enhancement in surface resistance, with the highest value observed at 0.1 g/L. More significantly, the incorporation of U-GO-ZnO leads to a substantial increase in $R_2$, reaching $6.02 \times 10^{-1}$, 1.30, and $7.80 \times 10^{-1}$ Ω. The maximum $R_2$ at 0.1 g/L U-GO-ZnO suggests the formation of a denser, more stable, and highly resistive passive layer, thereby providing superior corrosion protection.

## Discussion

### *The anti-corrosion performance from the weight-loss method*

Compared to the blank solution, only the corrosion rate after 30 days is higher (33.86 > 28.74 $mg.cm^{-2}.day^{-1}$). This result indicates that the anti-corrosion performance of U-GO-ZnO is limited up to 30 days of exposure. Similar to GO-ZnO, U-GO-ZnO exhibits an anti-corrosion effect only for 3, 5, and 10 days. At a higher concentration, the 0.2 g/L U-GO-ZnO solution shows effective anti−corrosion performance for up to 30 days with corrosion rates of 45.01, 35.93, 29.23, and 26.84 $mg.cm^{-2}.day^{-1}$, respectively.

### *Study of anti-corrosion performance using the kinetic potentiodynamic polarization method*

After 30 min, the potentiodynamic polarization curve of GOST 380-89 steel electrode in 3.5 wt.% NaCl solution containing GO-ZnO tends to shift to a more positive potential (Fig. 3a). Then, it shifted to a more negative potential after 60 min. After 120 min, the potentiodynamic polarization curves measured 0.05 GO-ZnO and 0.2 GO-ZnO solutions shifted to a more positive potential while 0.1 GO-ZnO still remained at a more negative potential. O. L. Riggs Jr. classified inhibitors into three types according to the shift of corrosion potential: anode type, cathode type, and mixed type (Olen & Riggs, 1973). If the difference between $\Delta E_{corr} = |E_{corr} - E^0_{corr}|$ is lower than 85 mV, the inhibitor belongs to the mixed group. Therefore, the results in Figure 5 and Table 2 show that GO-ZnO made an insignificant shift of the $E_{corr}$.

The potentiodynamic polarization method was performed on the steel electrode in NaCl solution in the presence of GO-ZnO and U-GO-ZnO which was shown in Figure 3. Compared to the blank sample ($E^0_{corr}$ = -848 mV vs. Ag/AgCl (KCl)), it is less than 85 mV, so they belong to the mixed-type inhibitor. The $E_{corr}$ of steel in solutions containing 0.05 and 0.2 g/L GO-ZnO has shifted to the right with a difference greater than 85 mV, which are -711 and -720 mV vs. Ag/AgCl (KCl), respectively, so this is an anode inhibitor. Compared to the blank sample ($E^0_{corr}$ = -852 mV vs. Ag/AgCl (KCl)), the $E_{corr}$ of steel in 3.5 wt.% NaCl solution has 0.05, 0.1, and 0.2 g/L of GO-ZnO are both less than 85 mV, so they belong to the mixed-type inhibitor. In addition, when the exposure time increases to 120 min, the $E_{corr}$ of steel in 3.5 wt.% NaCl solution with 0.05 and 0.1 g/L of GO-ZnO are lower than the blank sample ($E^0_{corr}$ = -723 mV vs. Ag/AgCl (KCl) and both differences are less than 85 mV, so they belong to the mixture type. However, the $E_{corr}$ of steel in a solution containing 0.2 g/L GO-ZnO has a difference greater than 85 mV, specifically -643 mV vs. Ag/AgCl (KCl), and shifts to the right of the blank, so this is an anode inhibitor.

The corrosion inhibition efficiencies calculated from the $i_{corr}$ values in Table 2 are 51.03% and 15.72%, respectively. These results indicate that GO-ZnO at concentrations of 0.05, 0.1, and 0.2 g/L predominantly acts as a cathodic inhibitor. From the above results, 0.05 g/L GO-ZnO exhibits the highest corrosion inhibition efficiency, which is 51.03%, 30.37%, and 56.15% after 30, 60, and 120 min, respectively. The results of investigating the effect of electrode exposure time in 3.5 wt.% NaCl solution with GO-ZnO show that a concentration of 0.05 g/L provides the highest corrosion inhibition efficiency. The potentiodynamic polarization curve of the steel electrode after 30, 60, and 120 min of immersion in a solution containing GO-ZnO is shown in Figure 4. The potentiodynamic polarization curve of the steel electrode exposed to the GO-ZnO solution for 30 min tends to shift to a more positive potential compared to the blank solution, whereas they shift toward more negative potentials after 60 min and 120 min.

The corrosion inhibition efficiencies calculated from $i_{corr}$ values in Table 3 are 63.72%, 32.71%, and 30.39%, respectively. However, after 60 and 120 min of exposure, the 0.1 g/L U-GO-ZnO solution provided corrosion inhibition efficiencies of 50.79% and 83.22%, respectively. After 60 min, the performance difference between 0.05 g/L GO-ZnO and 0.05 g/L U-GO-ZnO is not much, proving that at this concentration, modification with urea has increased corrosion protection for steel.

The slope coefficients $\beta_c$ and $\beta_a$, calculated from the potentiodynamic polarization curve, change to different degrees in the presence of materials

in NaCl solution. According to Dwivedi et al., (2022), it is shown that if the $\beta_c$ coefficient changes, the inhibitor affects the kinetics of the $H_2$ escape reaction. Besides, the change in $\beta_a$ value can come from the adsorption reaction of inhibitor molecules or $Cl^-$ ions on the metal surface (Dwivedi *et al.*, 2022). Tafel extrapolation results from Table 2 show that the polarization curve of steel in 0.05 g/L GO-ZnO solution at 30 and 120 minutes has $\beta_c$ and $\beta_a$ both decreasing compared to the blank sample, showing that this solution influences both cathodic and anodic reactions; with a more pronounced effect on the cathodic reaction. Therefore, it not only creates a film to protect the anode from the electrolyte solution, but also can control the evolution of $H_2$ at the cathode.

From the above results, GO-ZnO at a concentration of 0.05 g/L exhibits the highest corrosion inhibition efficiency, whereas U-GO-ZnO at 0.2 g/L does not exhibit a significant corrosion inhibition effect on the steel sample, which may be attributed to the incomplete dispersion of the material in the solution during the investigated exposure times. This indicates that, under these conditions, the material does not enhance and may even reduce the corrosion resistance. In addition, 0.05 g/L U-GO-ZnO exhibits a corrosion inhibition efficiency of 68.99% at 60 min, which is comparable to that of 0.05 g/L GO-ZnO, while 0.1 g/L U-GO-ZnO shows effective inhibition at an exposure time of 120 min. Although urea modification does not yield a higher corrosion inhibition efficiency than that of 0.05 g/L GO-ZnO, urea enhances the dispersion of the material within the coating matrix, whereas GO-ZnO tends to agglomerate.

***Evaluation of corrosion inhibition performance using electrochemical impedance spectroscopy (EIS)***

As shown in Figure 5a, all Nyquist plots exhibit a single semicircular arc in the high-frequency region, indicating that the corrosion process is predominantly controlled by charge transfer without the presence of additional diffusion-controlled processes. This behavior confirms the formation of an adsorbed layer of GO-ZnO and U-GO-ZnO on the steel surface, acting as a protective barrier layer that suppresses corrosion reactions. Notably, within the U-GO-ZnO series, the 0.1 g/L sample displays the largest Nyquist diameter, corresponding to the highest charge transfer resistance. However, further increasing the concentration to 0.2 g/L results in a decrease in the semicircle diameter. This trend suggests that an optimal concentration (0.1 g/L) promotes effective adsorption and uniform surface coverage, forming a compact protective barrier layer. At higher concentrations, possible aggregation of U-GO-ZnO may reduce adsorption efficiency and surface homogeneity, thereby diminishing the protective performance in 3.5 wt.% NaCl solution. The results of electrochemical parameter analysis based on the equivalent circuit diagram in Fig. 5d are presented in Table 4.

***Corrosion inhibition mechanism of GO-ZnO and U-GO-ZnO***

The corrosion inhibition mechanism of steel in 3.5 wt.% NaCl solution by GO-ZnO and U-GO-ZnO involves coupled electrochemical reactions and surface adsorption processes. In the absence of inhibitors, steel undergoes anodic dissolution:

$$Fe \rightarrow Fe^{2+} + 2e^- \quad (3)$$

while the cathodic reaction in aerated conditions is:

$$O_2 + 2H_2O + 4e^- \rightarrow 4OH^- \quad (4)$$

these processes lead to the formation of corrosion products:

$$Fe^{2+} + 2OH^- \rightarrow Fe(OH)_2 \rightarrow Fe_2O_3/Fe_3O_4 \quad (5)$$

When GO-ZnO is introduced, its nanosheets adsorb onto the steel surface via interactions between oxygen-containing functional groups (–OH, –COOH) and Fe atoms. This adsorption forms a protective barrier layer that blocks active corrosion sites, thereby reducing both anodic and cathodic reactions. In addition, ZnO nanoparticles contribute to stabilizing the adsorbed layer and promoting the formation of a more compact passive oxide layer.

The corrosion inhibition efficiency is further enhanced with U-GO-ZnO due to urea functionalization. The presence of $–NH_2$ and –CONH– groups significantly increases adsorption strength through coordination bonding and hydrogen interactions with the steel

surface. As a result, a denser, more uniform, and more stable protective barrier layer is formed. This layer effectively suppresses charge transfer, limits $Cl^-$ penetration, and stabilizes the passive layer. Consequently, U-GO-ZnO exhibits superior corrosion inhibition performance compared to GO-ZnO, demonstrating the clear advantage of urea modification in aggressive chloride environments.

## Conclusion

GO-ZnO and urea-functionalized GO-ZnO (U-GO-ZnO) nanocomposites were successfully synthesized and evaluated as corrosion inhibitors for mild steel in 3.5 wt.% NaCl solution. The results confirm that both materials exhibit effective corrosion inhibition behavior, which strongly depends on concentration, dispersion state, and exposure time.

GO-ZnO at a concentration of 0.05 g/L showed effective inhibition performance, with inhibition efficiencies reaching approximately 56% after 120 min of immersion. Meanwhile, U-GO-ZnO demonstrated improved dispersion in the corrosive medium due to urea functionalization, resulting in enhanced inhibition performance at longer exposure times, with efficiencies up to approximately 83% at 0.1 g/L. However, a further increase in concentration (0.2 g/L) led to reduced effectiveness, which can be attributed to nanoparticle agglomeration and decreased surface coverage. Electrochemical impedance spectroscopy results support these findings, showing an increase in charge transfer resistance in the presence of the inhibitors. The Nyquist plots indicate that the corrosion process is predominantly controlled by charge transfer, and the addition of GO-ZnO-based materials leads to a noticeable enhancement in interfacial resistance, reflecting the formation of an adsorbed protective layer on the steel surface.

From a mechanistic perspective, the corrosion inhibition performance arises from a synergistic combination of surface adsorption and barrier effects. The layered structure of GO provides an effective physical barrier that hinders the diffusion of corrosive species such as $Cl^-$ ions toward the metal surface. Simultaneously, ZnO nanoparticles contribute to improving the dispersion of GO sheets, reducing aggregation and promoting a more uniform interfacial coverage. This combined effect leads to the formation of a relatively compact adsorbed layer, which increases the tortuosity of diffusion pathways and suppresses the transport of aggressive ions.

The incorporation of urea further enhances this behavior by introducing additional functional groups (–$NH_2$, –CONH–), which strengthen the interaction between the inhibitor and the steel surface through coordination and hydrogen bonding. As a result, a more stable and homogeneous protective layer can be formed, contributing to improved corrosion resistance over time. Overall, this study highlights the critical roles of dispersion control, surface functionalization, and interfacial adsorption in determining the corrosion inhibition performance of GO-based nanocomposites. The findings provide useful insights for the rational design of advanced nanomaterial-based corrosion inhibitors for applications in chloride-containing environments.

***Acknowledgements:*** *The study was financially supported by the Joint Vietnam-Russia Tropical Science and Technology Research Center (Ecolan T-1.1-5 project).*

***Data Availability Statement****: All relevant data supporting the findings of this study are included within the article and its supplementary materials.*

***Author contributions:*** *Do Tan Tai: First author, Corresponding author, conceptualizing, writing & editing the original manuscript; Antonov S.V.: Writing-review; Bezrukov N.P., Makarova V.V.: Science advisor; Nguyen Thi Thu Hien: Editing; Nguyen Kim Thanh, Tran Thi Truc Suong, Nguyen T. Thu Hien: Investigating and analysis; Duong Huynh Thanh Linh: Writing-experiment. Tran Boi An: Writing-experiment, editing manuscript.*

***Statement on the use of Generative AI:*** *Limited AI Use: The authors declare that Generative AI tools were not used to generate or edit the scientific content of this manuscript. Where AI tools were employed (grammar checking/formatting only), the authors have verified all content and take full responsibility for the final version.*

***Conflicts of interest statement:*** *The authors declare that there is no conflict of interest regarding the publication of this paper.*

## References

Aryanto, D., Hastuti, E., Taspika, M., Anam, K., Isnaeni, I., Widayatno, W. B., Wismogroho, A. S., Marwoto, P., Nuryadin, B. W., Noviyanto, A., & Sugianto, S. (2020). Characteristics and photocatalytic activity of highly c-axis-oriented ZnO thin films. *Journal of Sol-*

*Gel Science and Technology*, *96*(1), 226–235. https://doi.org/10.1007/s10971-020-05361-5

Bai, X., Zhang, J., Li, N., & Liu, Y. (2015). Facile functionalization of graphene oxide with ethylenediamine as a solid base catalyst for Knoevenagel condensation reaction. *Catalysis Communications*, *64*, 105–109. https://doi.org/10.1016/j.catcom.2015.02.003

Chen, J., Qiao, Y., Meng, F., & Wang, Y. (2022). Corrosion and degradation of materials. *Coatings*, *12*(7), 969. https://doi.org/10.3390/coatings12070969

Dwivedi, A., Bharti, P., & Shukla, S. K. (2022). Chemical and electrochemical study of the effect of soluble sulfonated polystyrene on mild steel interface in hydrochloric acid solution. *Gazi University Journal of Science*, *35*(3), 808–820. https://doi.org/10.35378/gujs.936620

El Maghrabi, H. H., Nada, E. A., Soliman, F. S., & Moustafa, Y. M. (2016). One-pot environmentally friendly nanocomposite synthesis of novel $TiO_2$ nanotubes on graphene sheets as an effective photocatalyst. *Egyptian Journal of Petroleum*, *25*, 575–584. https://doi.org/10.1016/j.ejpe.2015.12.004

George, J., & Ishida, H. A. (2018). Review on the very high nanofiller-content nanocomposites: Their preparation methods and properties with high aspect ratio fillers. *Progress in Polymer Science*, *86*, 1–39. https://doi.org/10.1016/j.progpolymsci.2018.07.001

Giannakopoulou, T., Todorova, N., Erotokritaki, A., & Plakantonaki, N. (2020). Electrochemically deposited graphene oxide thin film supercapacitors: Comparing liquid and solid electrolytes. *Applied Surface Science*, *528*, 146801. https://doi.org/10.1016/j.apsusc.2020.146801

He, Y., Boluk, Y., Pan, J., Ahniyaz, A., Deltin, T., & Claesson, P. M. (2019). Corrosion protective properties of cellulose nanocrystals reinforced waterborne acrylate-based composite coating. *Corrosion Science*, *155*, 186–194. https://doi.org/10.1016/j.corsci.2019.04.012

Miyaji, H., Kanemoto, Y., Hamamoto, A., & Shitomi, K. (2022). Sustained antibacterial coating with graphene oxide ultrathin film combined with cationic surface-active agents in a wet environment. *Scientific Reports*, *12*, 1–13. https://doi.org/10.1038/s41598-022-21205-4

Mohamed, S. S., Sherif, A. E., Mohamed, A., & Mohamed, A. S. (2021). Facile design of graphene oxide-ZnO nanorod-based ternary nanocomposite as a superhydrophobic and corrosion-barrier coating. *Colloids and Surfaces A: Physicochemical and Engineering Aspects*, *611*, 125793. https://doi.org/10.1016/j.colsurfa.2020.125793

Necolau, M. I., & Pandele, A. M. (2020). Recent advances in graphene oxide-based anticorrosive coatings: An overview. *Coatings*, *10*(12), 1217. https://doi.org/10.3390/coatings10121217

Nedal, Y., Abu-Thabit, A. T., & Makhlouf, A. S. H. (2015). Recent advances in nanocomposite coatings for corrosion protection applications. In *Handbook of Nanoceramic and Nanocomposite Coatings and Materials* (pp. 515–549). Butterworth-Heinemann.

Nguyen, P. T., Nguyen, T. A., Carriere, P., & Ngo, X. C. (2018). Nanocomposite coatings: Preparation, characterization, properties, and applications. *International Journal of Corrosion*, *2018*, 4957659. https://doi.org/10.1155/2018/4957659

Olen, J., & Riggs, L. (1973). Corrosion inhibitors. In C. C. Nathan (Ed.), *National Association of Corrosion Engineers* (p. 11). Houston, TX.

Sodeinde, K., Olusanya, S., & Lawal, O. (2022). Enhanced adsorptional-photocatalytic degradation of chloramphenicol by reduced graphene oxide-zinc oxide nanocomposite. *Scientific Reports*, *12*, 1–13. https://doi.org/10.1038/s41598-022-10815-0

Wang, D., Zhao, J., Claesson, P., Zhang, F., Pan, J., & Shi, Y. (2024). Green synergy: Eco-friendly, high-performance anti-corrosion and wear-resistant coatings utilizing organosolv lignin and polydimethylsiloxane. *Progress in Organic Coatings*, *190*, 108365. https://doi.org/10.1016/j.porgcoat.2023.108365

Yang, D., Velamakanni, A., Bozoklu, G., Park, S., & Stoller, M. (2009). Chemical analysis of graphene oxide films after heat and chemical treatments by X-ray photoelectron and micro-Raman spectroscopy. *Carbon*, *47*(1), 145–152. https://doi.org/10.1016/j.carbon.2008.09.045